Article

Lanthanide-based Coordination Polymers for the Size-selective Detection of Nitroaromatics

Sumit Srivastava, Bipin Kumar Gupta, and Rajeev Gupta

Cryst. Growth Des., **Just Accepted Manuscript** • Publication Date (Web): 05 Jun 2017

Lanthanide-based Coordination Polymers for the Size-selective Detection of Nitroaromatics

Sumit Srivastava,[a] Bipin Kumar Gupta[b] and Rajeev Gupta*[a]

[a]Department of Chemistry, University of Delhi, Delhi-110007, India
[b]CSIR-National Physical Laboratory (CSIR), Dr K S Krishnan Road, New Delhi-110012, India

ABSTRACT: Lanthanide coordination polymers (LnCPs), $[Eu(HL)_3(CH_3OH)_2]_n$ (**1**) and $[Tb(HL)_3(CH_3OH)(H_2O)]_n \cdot H_2O$ (**2**) (H_2L = 3-(picolinamido)benzoic acid)), have been synthesized and characterized. Single crystal analyses of both LnCPs display that HL ligands not only coordinate to Ln ions but also act as the bridge between them generating 1D chains. Such 1D chains further pack into 3D architectures by the mediation of H-bonding interactions. Both LnCPs offer strategically placed exposed Lewis basic sites which potentially interact with the electron-deficient nitroaromatics whereas H-bonded 3D architecture having hydrophobic channels allows their facile inclusion within the network. A notable feature is the size-dependent sensing of nitroaromatics potentially governed by the packing of 1D chains into a 3D architecture. Both LnCPs act as the fluorescent sensor for quick, sensitive and selective detection of nitrobenzene not only in solution but also in the vapour phase suggesting potential applications in the sensing devices for the detection of nitroaromatics.

Introduction

Coordination polymers (CPs)[1-4] are a unique class of materials that have shown wide variety of notable applications.[5-18] Such applications are attributed to their highly crystalline nature, well-defined pores and channels, and the presence of functional sites such as open metal sites, acidic, and basic sites. These features have assisted in developing significant materials for sorption,[5,6] separation,[7] heterogeneous catalysis[8-14] as well as sensing[15,16] and recognition[17,18] applications. Among diverse CPs, luminescent coordination polymers offer noteworthy applications in sensing, recognition and binding events with guests and/or substrates.[15-19] Under this category, the ones based on lanthanide metals, i.e., lanthanide coordination polymers (LnCPs) are particularly interesting materials for their ability to respond to guests and/or substrates in the form of large optical signal.[20,21] LnCPs based materials with open metal sites,[22,23] hydrogen bonding (H-bonding) sites[24,25] and exposed Lewis basic sites[26-29] have been particularly successful for the recognition of small molecules as well as cations.[30-39]

Nitroaromatics are toxic compounds used extensively as the explosives[32-39] and as the starting materials in various industrially and commercially important products such as dyes, pesticides, polyurethane foams, and polymers.[40-43] Nitroaromatics are obstinate to biological treatment and remain in the biosphere, where they constitute a source of pollution due to both toxic and mutagenic effects on microorganisms, aquatic and other organisms, as well as humans.[44-49] Exposure of nitroaromatics to humans, particularly the volatile ones, can cause serious health hazards such as cancer, liver damage and kidney failure.[44-49] Therefore, detection of nitroaromatics is a compelling requirement not only due to their explosive qualities but also due to their environmental hazardous impact.[39-49] Although nitroaromatics exhibit strong UV absorption but their low fluorescence render their direct detection impractical.[32-39] Such a problem necessitates the use of an alternate strategy and therefore several sensors have been developed for the detection of nitroaromatics.[23-59] In this context, electron-rich sensors have been particularly notable considering the electron-deficient nature of nitroaromatics.[15-21,24-39] In this work, we present luminescent one-dimensional (1D) Eu^{3+} and Tb^{3+} based LnCPs which transform into three-dimensional (3D) architecture held together by H-bonding interactions for the detection of nitroaromatics. We illustrate that both LnCPs offering well-defined pores and channels allow selective detection of smaller nitroaromatics whereas their 3D polymeric nature enables heterogeneous sensing of nitroaromatics both in the solution as well as in the vapor phase.

Experimental Section

Materials and Methods. Reagents of analytical grade were procured from Sigma-Aldrich, Alfa-Aesar, and Spectrochem and were used without further purification. The solvents were purified using standard literature methods.[50] 2-(3-Ethylbenzoate-carbomyl)pyridine (**HL1**) was synthesized as reported in the litrature.[51]

Synthesis of Ligand H_2L

2-(3-Ethylbenzoate-carbomyl)pyridine (**HL1**) (1 g, 3.7 mmol) was dissolved in a mixture of THF/H_2O (3:1, v/v) and treated with 3 equiv. of NaOH. The reaction mixture was stirred for 12 h at room temperature. The resulting solution was neutralized by using 3 N HCl. Removal of THF under vacuum resulted in the precipitation of a product which was re-dissolved by

adding ethyl acetate. The ethyl acetate layer was separated and dried over anhyd. Na_2SO_4. Slow evaporation of ethyl acetate solution at room temperature produced a highly crystalline product within 2-3 d which was filtered and dried under vacuum. Yield: 0.75 g (84 %). Anal. Calcd. for $C_{13}H_{10}N_2O_3$: C, 64.46%; H, 4.16%; N, 11.56%. Found: C, 64.62%; H, 4.38%; N, 11.54%. ^{1}H NMR spectrum (DMSO-d_6, 400 MHz; Figure S1, SI): δ = 13.00 (s, 1H, COOH), 10.81 (s, 1H, CONH), 8.05-8.02 (d, 2H, H3/H5), 7.47-7.43 (t, 1H, H4), 8.59 (s, 1H, H7), 8.14-8.13 (d, 1H, H10), 7.68-7.63 (m, 2H, H11/H12), 8.71–8.70 (d, 1H, H13). ^{13}C NMR spectrum (DMSO-d_6, 100 MHz; Figure S2, SI): δ = 167.73 (C1), 129.41 (C2), 125.18 (C3), 131.82 (C4), 127.57 (C5), 138.71 (C6), 121.65 (C7), 163.33 (C8), 150.23 (C9), 123.03 (C10), 139.14 (C11), 125.30 (C12), 148.97 (C13). FTIR spectrum (Zn-Se ATR, selected peaks; Figure S3, SI): 3332 (N-H_{amide}), 2920 (O-H_{acid}), 1700 (asymmetric C=O_{acid}), 1666 (symmetric C=O_{acid}), 1594 (C=O_{amide}) cm^{-1}.

Synthesis of $[Eu(HL)_3(CH_3OH)_2]_n$ (LnCP 1)

Solid $Eu(NO_3)_3.5H_2O$ (0.059 g, 0.14 mmol) was added to a solution containing ligand **H_2L** (0.1 g, 0.42 mmol) and ET_3N (0.043 g, 0.42 mmol) in CH_3OH (10 ml) and the reaction mixture was stirred for 1 h. A white product was obtained which was filtered and dried under vacuum. Crystallization was achieved by the vapour diffusion of diethyl ether to a DMF solution of the crude product at room temperature which afforded a highly crystalline product within 2-3 d. Yield: 0.111 g (85%). Anal. Calcd. for $C_{41}H_{35}N_6O_{11}Eu$: C, 52.40%; H, 3.75%; N, 8.94%. Found: C, 52.57%; H, 3.48%; N, 8.75%. FTIR spectrum (Zn-Se ATR, selected peaks): ν = 3332 (N-H_{amide}), 1680 (asymmetric C=O_{acid}), 1635 (symmetric C=O_{acid}), 1595 (C=O_{amide}), 1393 (C=N) cm^{-1}.

Synthesis of $[(Tb(HL)_3(CH_3OH)(H_2O)]_n \bullet H_2O$ (LnCP 2)

This compound was synthesized in a similar manner with an identical scale as mentioned for **1** except using $Tb(NO3)_3.5H_2O$ in place of $Eu(NO_3)_3.5H_2O$. Yield 0.090 g (70%). Anal. Calcd. for $C_{40}H_{35}N_6O_{12}Tb$: C, 50.54%; H, 3.71%; N, 8.84%. Found: C, 50.55%; H, 3.60%; N, 8.78%. FTIR spectrum (Zn-Se ATR, selected peaks): ν = 3330 (N-H_{amide}), 1674 (asymmetric C=O_{acid}), 1630 (symmetric C=O_{acid}), 1594 (C=O_{amide}), 1390 (C=N) cm^{-1}.

Physical Methods. The FTIR spectra (Zn-Se ATR, 4000–400 cm^{-1}) were recorded with a Perkin-Elmer Spectrum-Two spectrometer having Ze-Se ATR. The NMR spectroscopic measurements were carried out with a Jeol 400 MHz spectrometer. The absorption spectra were recorded with either Perkin-Elmer Lambda 25 or Lambda 35 spectrophotometers. The elemental analysis data were obtained with an Elementar Analysen Systeme GmbH Vario EL-III instrument. Thermal gravimetric analysis (TGA) was performed with a DTG 60 Shimadzu at 5 °C min^{-1} heating rate under the dinitrogen atmosphere. X-ray powder diffraction (XRPD) studies were performed either with an X'Pert Pro from Panalytical or a Bruker AXS D8 Discover instrument (Cu Kα radiation, λ = 1.54184 Å). The samples were ground and subjected to the range of θ = 5-50 with slow scan rate at room temperature. Scanning electron microscopic (SEM) measurements were performed with a Jeol SM 6610 LV instrument. Luminescence measurements were made either with an Edinburgh Instrument FLS 900 luminescence spectrometer or Cary Eclipse Fluorescence Spectrophotometer.

Single Crystal Structure Determination. Single crystals suitable for the X-ray diffraction studies were grown by the diffusion of diethyl ether vapours to a DMF solution of the corresponding product. The intensity data were collected at 293 K with an Oxford XCalibur CCD diffractometer equipped with a graphite monochromatic Mo-Kα radiation (λ = 0.71073 Å).[52] An empirical absorption correction was applied using the spherical harmonics implemented in the SCALE3 ABSPACK scaling algorithm.[52] The structures were solved by direct methods using SIR-92[53] and refined by the full-matrix least-squares refinement techniques on F^2 using the program SHELXL-97[54] in the WinGX module.[55] All hydrogen atoms were fixed at the calculated positions with isotropic thermal parameters whereas all non-hydrogen atoms were refined anisotropically. For LnCP **1**, some unassigned electron density was noted very close to the Eu atom (< 1Å) due to the absorption artifact. This resulted in an A-level alert in checkCIF. For LnCP **2**, A-level alert in checkCIF was due to the observation of short D…A contacts between the disordered water molecules (O1w and O2w). Details of the crystallographic data collection and structure solution parameters are provided in Table 1.

Fluorescence Experiments. 3 mg of a compound (**1** or **2**) was suspended in 3 ml of $CHCl_3$ and the suspension was sonicated for 1 h. The resultant suspension was used for PL studies to maintain the homogeneity of the suspended compound. This suspension was excited at 358 nm and the florescence spectra were recorded in the range of 450 nm – 750 nm. The quenching experiments were performed by the incremental addition of nitroaromatics to the aforementioned $CHCl_3$ suspension. To maintain the homogeneity, sample was sonicated before each run after the addition of nitro compounds.

Determination of Stern-Volmer constant (Ksv) and Detection limit.

Stern-Volmer constant (Ksv) were determined by using the Stern-Volmer equation (1) where I0 and I are the emission intensity in the presence and absence of quencher (Q), respectively while Ksv is the Stern-Volmer constant.[30-39] Detection limits were calculated by using equation (2) where σ is defined as the standard deviation of a blank sample and *k* represents the slop of the linear calibration plot.[30-39]

$Io/I = 1 + Ksv\,[Q]$ ..... (1)

Detection limit = $3\sigma/k$ ..... (2)

Results and Discussion

Synthesis and Characterization

The ligand **H_2L**, offering both carboxylic acid and pyridine-2-carboxamide functional groups, was utilized for the synthesis of LnCPs. We anticipated that Ln(III) metals would preferentially coordinate via $O_{carboxylate}$ groups due to their strong ox-

ophillic nature[56] leaving pyridine-2-carboxamide groups unligated. The reaction of **H_2L** with $M(NO_3)_3 \bullet 5H_2O$ (M = Eu^{3+} or Tb^{3+}) in presence of Et_3N in CH_3OH produced LnCPs, $[Eu(HL)_3(CH_3OH)_2]_n$ (**1**) and $[(Tb(HL)_3(CH_3OH)(H_2O)]_n \bullet H_2O$ (**2**) (Scheme 1). Both **1** and **2** were crystallized by the diffusion of diethyl ether vapours to a DMF solution of the respective product.

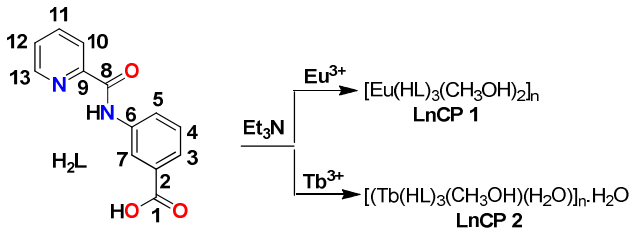

Scheme 1. Ligand **H_2L** and its lanthanide coordination polymers (LnCP) **1** and **2**.

The FTIR spectra of LnCPs **1** and **2** exhibited red-shifted asymmetric as well as symmetric ν_{COO} stretches at 1674-1680 and 1630-1635 cm^{-1}, respectively when compared with the free ligand **H_2L** (Figures S3 and S4; SI). On the other hand, nearly unchanged amidic C=O bands were noted at ca. 1595 cm^{-1}. These observations suggest that the Ln^{3+} ions are coordinated to the arylcarboxylate groups and not to the amidic-O groups. In addition, a sharp band at ca 3330 cm^{-1} was due to the $\nu_{N\text{-}H}$ stretch of the pyridine-2-carboxamide fragment. Thermogravimetric analysis (TGA) was performed on both **1** and **2** in the temperature range of 35-180 ˚C to shed light on the nature of lattice as well as coordinated solvent molecules, decomposition profile and thermal stability of LnCPs. TGA plots show ca. 7% weight loss for the release of lattice as well as coordinated solvent molecules.[57] TGA plots further exhibit that both LnCPs are stable up to ca. 400˚C (Figure S5; SI).

Crystal Structures

To understand the solid-state structure and conformation, ligand **H_2L** as well as both LnCPs were crystallographically characterized (Tables 1 and S1-S4, SI). The ligand **H_2L** crystallized in monoclinic space group $P2_1/n$. Herein, two arene rings are almost co-planer to each other as revealed by a small dihedral angle of ca. 5.8˚. Interestingly, ligand **H_2L** exhibited H-bonding based self-assembly where -OH of the carboxylic acid functions as the hydrogen bond (H-bond) donor whereas appended N-pyridyl group acted as the H-bond acceptor (Figure 1). Topological analysis[58,59] of H-bonding based self-assembly illustrate that the structure is consist of (0 1 0) chain with point symbol of net (4^2.6).

Crystal Structures of LnCPs

Single crystal X-ray analysis reveals that the isostructural LnCPs **1** and **2** crystalize in monoclinic cell with $P2_1/c$ space group. The asymmetric unit of **1** and **2** contains one Ln^{3+} ion (Ln = Eu and Tb), three mono-anionic **HL** ligands and two coordinated solvent molecules (methanol and/or water) (Figure 2a). The structures of LnCPs **1** and **2** display that ligands bridge Ln^{3+} ions in such a way so as to generate a 1D polymeric chain propagating along the *b*-axis (Figure 2b). The angle between any three Ln^{3+} ions, in a 1D chain, is ca. 174.5° suggesting that the metals are almost linearly arranged. Such a fact further justifies the 1D nature of both LnCPs. In both LnCPs, any Ln^{3+} ion is eight-coordinated (Figure 2c). In LnCP **1**, two Eu^{3+} ions are bridged by two arylcarboxylate groups from two ligands in *syn,syn*-$\eta^1:\eta^1:\mu_2$ bridging mode while every Eu^{3+} ion is further coordinated by a carboxylate group in a bidentate chelating mode in addition to two CH_3OH molecules (Figure 2c). LnCP **2** displays an identical coordination environment around a Tb^{3+} ion except that two terminal sites are ligated by a water and a methanol molecule. Interestingly, in both LnCPs **1** and **2**, pyridine-2-carboxamide fragment of a ligand remains uncoordinated (Figure 2b and 2d).

The 1D chains are packed in parallel fashion involving $C{=}O_{amide}\cdots H\text{-}C_{arene}$ H-bonding interactions and thus generating a 3D architecture (Figure 2e). A perspective view of LnCP **1** clearly illustrates the presence of channels propagating along the *c*-axis (Figure 2f). Similarly, LnCP **2** displays the presence of channels as a result of generation of 3D network due to the $C{=}O_{amide}\cdots H\text{-}C_{arene}$ H-bonding interactions (Figures 2g and 2h). Topological analysis[58,59] of LnCPs **1** and **2** illustrate that Eu^{3+}/Tb^{3+} ions functioned as the 4-connected nodes while ligands acted as the 2-connected linkers generating 1D chains with identical point symbol $(4^2)(4)_2$ (Figure 2i).

Photoluminescence Studies of LnCPs

The photoluminescence (PL) properties of both LnCPs were carried out at room temperature. The solid-state excitation and emission spectra of LnCPs **1** and **2** are illustrated in Figure 3. LnCP **1** displays an excitation band at 358 nm and characteristic emission bands of Eu^{3+} ion at 594, 617 (Intense band, red), 651, and 694 nm, which can be attributed to f-f $^5D_0 \rightarrow {}^7F_j$ (j = 1–4) transitions, respectively.[36] On the other hand, LnCP **2** exhibits emission bands for the Tb^{3+} ion at 487, 542 (Intense band, green), 581 and 620 nm, which can be assigned to f-f $^5D_4 \rightarrow {}^7F_j$ (j = 6, 5, 4 and 3) transitions, respectively.[25] The emission properties of both LnCPs were also studied in different solvents as their suspensions. For that purpose, LnCPs **1** and **2** were suspended in assorted solvents and their emission spectra were recorded by maintaining an effective concentration of 3 mg/3 ml. Both LnCPs **1** and **2** exhibited the highest emission intensity in $CHCl_3$ whereas lowest emission was noted in MeOH (Figure 4). As both LnCPs behaved nearly identical; **1** was selected as a model system for further studies in different solvents ($CHCl_3$, CH_2Cl_2, EtOAc, hexane, CH_3CN, $(CH_3)_2CO$, EtOH, THF, H_2O, and CH_3OH) as well as assorted reagents such as benzene, toluene, chlorobenzene, bromobenzene, phenol, aniline, benzaldehyde, nitrobenzene, nitroethane, 1-nitropropane, 2-nitropropane, and nitrocyclopentane. Importantly, maximum quenching in the emission intensity was caused by the electron-deficient species such as benzaldehyde and nitrobenzene (Figure 5a). On the other hand, aliphatic nitro reagents did not result in appreciable change in the emission intensity (Figure 5b).

Sensing of Nitroaromatics

PL studies in different solvents and reagents suggested that LnCP **1** functioned as a good sensor for the electron-deficient solvents and/or reagents as well as the ones containing nitro

group(s). Although no significant PL change was noted for nitroaliphatic compounds, maximum quenching was observed for the nitroaromatics (nitrobenzene, 4-nitrophenol, 1,3-dinitrobenzene, 1-nitronapthalene, 2,4,6-trinitrophenol, 3,5-dinitrosalicylic acid and 3,5-dinitrobenzyl chloride). Collectively, these results advocate that LnCPs **1** has strong affinity to sense assorted nitroaromatics although maximum quenching was noted for the smallest one, nitrobenzene (Figure 6).

Subsequently, PL studies of **1** as a $CHCl_3$ suspension, was studied with incremental addition of different nitroaromatics and percentage of quenching, Ksv values (from Stern–Volmer analysis), and detection limits were calculated (Figures 7a-7d and S6-S29 (SI); and Table 2). From these studies, following quenching efficiency trend was observed: nitrobenzene > 4-nitrophenol > 1,3-dinitrobenzene > 1-nitronapthalene > 2,4,6-trinitrophenol > 3,5-dinitrosalicylic acid > 3,5-dinitrobenzyl chloride. Importantly, such a trend is consistent with the order of the molecular sizes of these nitroaromatics and can be attributed to the ease in their diffusion abilities within the 3D network structure of coordination polymers (Figure 6, right panel and Table S5). The smallest nitrobenzene resulted in fast diffusion as well as unhindered accessibility to the interiors of the coordination polymer and therefore it caused maximum quenching in the emission intensity of LnCP **1**. For example, a ratio of quenching efficiencies of nitrobenzene and 1-nitronaphthalene yields 1.46 that closely matches to 1.57, a ratio of volumes of two substrates (*cf.* Tables 2 and S5, SI). Such a comparison convincingly infers that the sensing ability of the present LnCPs is a function of the molecular dimensions of the substrates.

Sensing of Nitrobenzene

The sensing performance of both LnCPs towards various nitroaromatics, particularly volatile nitrobenzene due to its smallest size is noteworthy as it belongs to a group of substances known as the volatile organic compounds (VOCs).[36-38] Hence, dependency of the degree of luminescence quenching on the concentration of nitrobenzene was examined. Such a study revealed that LnCP **1** is quite sensitive towards nitrobenzene even at very low concentrations. At around 1000 μM concentration of nitrobenzene, PL intensity is significantly quenched with a quenching yield of ca. 90% (Figure 7a and 7b). The Stern–Volmer analysis (*K*sv) and detection limit of LnCP **1** with nitrobenzene was found to be 2.38×10^4 and 49 μM, respectively (Figure 7c and 7d). These values illustrate that LnCp **1** has good sensitivity for detecting even small amount of nitrobenzene. In fact, such a noteworthy detection is superior to that of previously reported sensors for detecting nitrobenzene (*see* Table S6, SI for comparison with literature examples).[36-38] Similar results were obtained when LnCP **2** was used in place of **1** (entry 8, Table 2 and Figures S30-S33, SI). In this case as well, smaller nitroaromatics resulted in maximum quenching in comparison to bulkier nitroaromatics supporting various studies with LnCP **1**.

Vapor Phase Sensing of Nitrobenzene

The significant ability of both LnCPs **1** and **2** as a $CHCl_3$ suspension to sense nitrobenzene prompted us to study their capability to detect vapor-phase nitrobenzene at room temperature. In a typical experiment, vacuum-dried LnCP **1** was exposed to nitrobenzene vapors for a fixed period of time at room temperature followed by the measurement of its PL intensity. The fluorescence of **1** was considerably quenched within 4 h of exposure whereas maximum quenching was noted after a period of 12 h (Figure 7e and 7f). Such a fact is further evident by the sample's optical photographs under normal and UV light (Figure 7g-7i). These results are noteworthy and illustrate that LnCP **1** is also able to sense nitrobenzene vapors. Remarkably, **1** can be fully regenerated by simply washing with $CHCl_3$ a couple of times. In fact, its remarkable recyclability suggests its potential use for solid-state sensing applications as only a negligible drop in performance was noted even after five cycles (Figure S34, SI).

Possible Mechanism

In order to elucidate possible mechanism for the observed PL quenching by the nitroaromatics, powder XRD as well as scanning electron microscopy (SEM) was employed to monitor the structural and morphological changes during the sensing of nitrobenzene (Figure S35, SI). The powder XRD patterns of LnCP **1** immersed in nitrobenzene for 15 min and 1 h were identical to that of pristine **1**. Such a fact strongly suggests that the framework structure remains stable although photoluminescence is mostly quenched. Further support came from the SEM images that additionally inferred that the nitrobenzene has not caused any morphological changes to the LnCP **1** after 15 min and even 1 h of exposure of nitrobenzene (right panels; Figure S35, SI). It can be therefore concluded that PL quenching within a short period of time mainly results from the electron donor-acceptor mechanism between LnCPs and nitroaromatics.[19,36-39] We therefore propose that the uncoordinated pyridine-2-carboxamide fragments of LnCPs function as the Lewis basic sites and interact with electron-deficient nitroaromatics and such an interaction causes the PL quenching.

It is well known that nitroaromatics are electron-deficient molecules[19,39] whereas presence of planar aromatic ring allows facile intercalation or stacking.[36-39] It is suggested that once nitroaromatics are able to diffuse inside the channels present within the interior of the present LnCPs; energy transfer process from HL to the central Eu/Tb ions is forbidden, resulting in fluorescence quenching of LnCPs.[60] Importantly, both LnCPs **1** and **2** offer 3D network which is generated by the operation of H-bonding interactions. Therefore, size as well as shape of a potential substrate (i.e., nitroaromatics) will be a limiting factor that could be related to the pores and channels created by the H-bonding interactions. The facile diffusion of a smaller substrate (e.g., nitrobenzene) is likely to result in the maximum quenching as observed with the present LnCPs. In fact, such a proposal gets support from the solvent-dependent PL behavior of both LnCPs **1** and **2**. We believe that any solvent having ability to disrupt the H-bonding between 1D chains, responsible for the generation of 3D structure, is likely to affect the PL performance of LnCPs. Indeed, both LnCPs displayed significant solvent dependency and such a fact is related to the disruption of 3D structure as

a result of a solvent's polarity (e.g., MeOH) or its swelling efficiency (e.g, THF, CH_2Cl_2).[61]

Conclusions

In this work, two lanthanide coordination polymers (LnCPs) have been synthesized and characterized. Both LnCPs illustrated 1D chain-like structure which was further extended to 3D architecture due to the involvement of H-bonding interactions. Both LnCPs were successfully used for the sensing of various nitroaromatics although maximum emission quenching was noted for the smallest nitrobenzene. Both LnCPs offered strategically placed exposed Lewis basic sites which potentially interacted with the electron-deficient nitroaromatics whereas H-bonded 3D architecture having hydrophobic channels allowed their facile inclusion within the network. An important observation was the size-dependent sensing of nitroaromatics potentially governed by the packing of 1D chains into a 3D architecture. Importantly, vapor-phase detection of nitrobenzene as well as recyclability of LnCPs suggests their potential applications in the sensing devices for the detection of nitroaromatics.

ASSOCIATED CONTENT

Supporting Information. Figures for NMR, FTIR, and absorption spectra, TGA, titration plots, spectral fittings, powder XRD and SEM micrographs; and tables of bond distances, bond angles, H-bonding parameters; size and percentage quenching efficiency of nitroaromatics; and a comparative table with literature examples for the sensing of nitroaromatics. This material is available free of charge via the Internet at http://pubs.acs.org.

AUTHOR INFORMATION

Corresponding Author

*Fax: +91-11-27666605; Email: rgupta@chemistry.du.ac.in. Website: http://people.du.ac.in/~rgupta/.
ORCID: 0000-0003-2454-6705

Author Contributions

The manuscript was written through contributions of all authors.

Notes

The authors declare no competing financial interest.

ACKNOWLEDGMENT

RG acknowledges financial support from the Science and Engineering Research Board (SERB), New Delhi. SS thanks UGC, New Delhi for the SRF fellowship. Authors thank CIF-USIC of this university for the instrumental facilities including X-ray data collection and CSIR-NPL, New Delhi for the solid-state PL measurements.

REFERENCES

(1) Kumar, G.; Gupta, R. Molecularly designed architectures - the metalloligand way. *Chem. Soc. Rev.* **2013**, *42*, 9403-9453.
(2) Srivastava, S.; Gupta, R. Metalloligands to material: design strategies and network topologies. *CrystEngComm*, **2016**, *18*, 9185-9208.
(3) Cook, T. R.; Stang, P. J. Recent Developments in the Preparation and Chemistry of Metallacycles and Metallacages via Coordination. *Chem. Rev.* **2015**, *115*, 7001-7045.
(4) Schoedel, A.; Li, M.; Li, D.; O'Keeffe, M.; Yaghi, O. M. Structures of Metal-Organic Frameworks with Rod Secondary Building Units. *Chem. Rev.* **2016**, *116*, 12466−12535.
(5) Kumar, K. V.; Preuss, K.; Titirici, M.-M.; Rodríguez-Reinoso, F. Nanoporous Materials for the Onboard Storage of Natural Gas. *Chem. Rev.* **2017**, *117*, 1796−1825.
(6) Maspoch, D.; Ruiz-Molina, D.; Veciana, J. Old materials with new tricks: Multifunctional open-framework materials. *Chem. Soc. Rev.***2007**, *36*, 770-818.
(7) Li, J. R.; Kuppler, R. J.; Zhou, H. C. Selective gas adsorption and separation in metal-organic frameworks. *Chem. Soc. Rev.* **2009**, *38*, 1477-1504.
(8) Srivastava, S.; Kumar, V.; Gupta R. A Carboxylate-Rich Metalloligand and Its Heterometallic Coordination Polymers: Syntheses, Structures, Topologies, and Heterogeneous Catalysis. *Cryst. Growth Des.* **2016**, *16*, 2874-2886.
(9) Srivastava, S.; Aggarwal, H.; Gupta, R. Three-Dimensional Heterometallic Coordination Networks: Syntheses, Crystal Structures, Topologies, and Heterogeneous Catalysis. *Cryst. Growth Des.* **2015**, *15*, 4110-4122.
(10) Singh, A. P.; Ali, A.; Gupta, R. Cobalt complexes as the building blocks: $\{Co^{3+}–Zn^{2+}\}$ heterobimetallic networks and their properties. *Dalton Trans.* **2010**, *39*, 8135-8138.
(11) Singh, A. P.; Kumar, G.; Gupta, R. Two-dimensional $\{Co^{3+}–Zn^{2+}\}$ and $\{Co^{3+}–Cd^{2+}\}$ networks and their applications in heterogeneous and solvent-free ring opening reactions. *Dalton Trans.* **2011**, *40*, 12454-12461.
(12) Kumar, G.; Gupta, R. Cobalt Complexes Appended with p- and m-Carboxylates: Two Unique $\{Co^{3+}–Cd^{2+}\}$ Networks and Their Regioselective and Size Selective Heterogeneous Catalysis. *Inorg. Chem.* **2012**, *51*, 5497-5499.
(13) Kumar, G.; Gupta, R. Three-Dimensional $\{Co^{3+}–Zn^{2+}\}$ and $\{Co^{3+}–Cd^{2+}\}$ Networks Originated from Carboxylate-rich Building Blocks: Syntheses, Structures, and Heterogeneous Catalysis. *Inorg. Chem.* **2013**, *52*, 10773-10787.
(14) Kumar, G.; Kumar, G.; Gupta, R. Manganese- and Cobalt-Based Coordination Networks as Promising Heterogeneous Catalysts for Olefin Epoxidation Reactions. *Inorg. Chem.* **2015**, *54*, 2603-2615.
(15) Zhou, X.; Lee, S.; Xu, Z.; Yoon, J. Recent Progress on the Development of Chemosensors for Gases. *Chem. Rev.* **2015**, *115*, 7944-8000.
(16) Wagner, T.; Haffer, S.; Weinberger, C.; Klaus, D.; Tiemann, M. Mesoporous Materials as Gas Sensors. *Chem. Soc. Rev.* **2013**, *42*, 4036
(17) Chen, B.; Xiang, S.; Qian, G. Metal-Organic Frameworks with Functional Pores for Recognition of Small Molecules. *Acc. Chem. Res.* **2010**, *43*, 1115-1124.
(18) Chen, B.; Wang, L.; Zapata, F.; Qian, G.; Lobkovsky, E. B. A Luminescent Microporous Metal-Organic Framework for the Recognition and Sensing of Anions. *J. Am. Chem. Soc.,* **2008**, *130*, 6718-6719.
(19) Hu, Z. C.; Deibert, B. J.; Li, J. Luminescent Metal-Organic Frameworks for Chemical Sensing and Explosive Detection. *Chem. Soc. Rev.* **2014**, *43*, 5815-5840.
(20) Guo, Z.; Xu, H.; Su, S.; Cai, J.; Dang, S.; Xiang, S.; Qian, G.; Zhang, H.; O' Keeffe, M.; Chen, B. A robust near infrared luminescent ytterbium metal–organic framework for sensing of small molecules. *Chem. Commun.*, **2011**, *47*, 5551-5553.
(21) Salinas, Y.; M.-M., R.; Marcos, M. D.; Sancenon, F.; Costero, A. M.; Parra, M.; Gil, S. Optical chemosensors and reagents to detect explosives. *Chem. Soc. Rev.*, **2012**, *41*, 1261-1296.
(22) Chen, B.; Yang, Y.; Zapata, F.; Lin, G.; Qian, G.; Lobkovsky, E. B. Luminescent Open Metal Sites within a Metal-Organic Frame-

work for Sensing Small Molecules. *Adv. Mater.*, **2007**, *19*, 1693-1696.

(23) Zhang, Z.; Xiang, S.; Rao, X.; Zheng, Q.; Fronczek, F. R.; Qian, G.; Chen, B. A rod packing microporous metal–organic framework with open metal sites for selective guest sorption and sensing of nitrobenzene. *Chem. Commun.*, **2010**, *46*, 7205-7207.

(24) Wang, Z.-J.; Qin, L.; Chen, J.-X.; Zheng, H.-G. H⁻ Bonding Interactions Induced Two Isostructural Cd(II) Metal-Organic Frameworks Showing Different Selective Detection of Nitroaromatic Explosives. *Inorg. Chem.* **2016**, *55*, 10999-11005.

(25) Pal, S.; Bharadwaj, P. K. A Luminescent Terbium MOF Containing Hydroxyl Groups Exhibits Selective Sensing of Nitroaromatic Compounds and Fe(III) Ions. *Cryst. Growth Des.* **2016**, *16*, 5852-5858.

(26) Joarder, B.; Desai, A. V.; Samanta, P.; Mukherjee, S.; Ghosh, S. K. Selective and Sensitive Aqueous-Phase Detection of 2,4,6- Trinitrophenol (TNP) by an Amine-Functionalized Metal–Organic Framework. *Chem. Eur. J.* **2015**, *21*, 965-969.

(27) Mukherjee, S.; Desai, A. V.; Manna, B.; Inamdar, A. I.; Ghosh, S. K. Exploitation of Guest Accessible Aliphatic Amine Functionality of a Metal−Organic Framework for Selective Detection of 2,4,6-Trinitrophenol (TNP) in Water. *Cryst. Growth Des.* **2015**, *15*, 4627-4634.

(28) Nagarkar, S. S.; Desai, A. V.; Samanta, P.; Ghosh, S. K. Aqueous phase selective detection of 2,4,6-trinitrophenol using a fluorescent metal-organic framework with a pendant recognition site. *Dalton Trans.*, **2015**, *44*, 15175-15180.

(29) Tang, Q.; Liu, S.; Liu, Y.; Miao, J.; Li, S.; Zhang, L.; Shi, Z.; Zheng, Z. Cation Sensing by a Luminescent Metal-Organic Framework with Multiple Lewis Basic Sites. *Inorg. Chem.* **2013**, *52*, 2799-2801.

(30) Hao, Z.; Song, X.; Zhu, M.; Meng, X.; Zhao, S.; Su, S.; Yang, W.; Song, S.; Zhang, H. One-dimensional channel-structured Eu-MOF for sensing small organic molecules and Cu^{2+} ion. *J. Mater. Chem. A,* **2013**, *1*, 11043-11050.

(31) Zhu, Y.-M.; Zeng, C.-H.; Chu, T.-S.; Wang, H.-M; Yang, Y.-Y.; Tong, Y.-X.; Su, C.-Y.; Wong, W.-T. A novel highly luminescent LnMOF film: a convenient sensor for Hg^{2+} detecting. *J. Mater. Chem. A*, **2013**, *1*, 11312-11319.

(32) Gole, B.; Bar, A. K.; Mukherjee, P. S. Fluorescent metal–organic framework for selective sensing of nitroaromatic explosives. *Chem. Commun.*, **2011**, *47*, 12137-12139.

(33) Hu, X.-L.; Liu, F.-H.; Qin, C.; Shao, K.-Z.; Su, Z.-M. A 2D bilayered metal–organic framework as a fluorescent sensor for highly selective sensing of nitro explosives. *Dalton Trans.*, **2015**, 44, 7822-7827.

(34) Zhou, X.; Li, H.; Xiao, H.; Li, L.; Zhao, Q.; Yang, T.; Zuo, J.; Huang, W. A microporous luminescent europium metal-organic framework for nitro explosive sensing. *Dalton Trans.*, **2013**, *42*, 5718-5723.

(35) Banerjee, D.; Hu, Z.; Li, J. Luminescent metal-organic frameworks as explosive sensors. *Dalton Trans.*, **2014**, *43*, 10668-10685.

(36) Gao, R.-C.; Guo, F.-S.; Bai, N.-N.; Wu, Y.-L.; Yang, F.; Liang, J.-Y.; Li, Z.-J.; Wang, Y.-Y. Two 3D Isostructural Ln(III)-MOFs: Displaying the Slow Magnetic Relaxation and Luminescence Properties in Detection of Nitrobenzene and $Cr_2O_7^{2-}$. *Inorg. Chem.* **2016**, *55*, 11323-11330.

(37) Xia, Y.-P.; Li, Y.-W.; Li, D.-C.; Yao, Q.-X.; Du, Y.-C.; Dou, J.-M. A new Cd(II)-based metal–organic framework for highly sensitive fluorescence sensing of nitrobenzene. *CrystEngComm*, **2015**, 17, 2459-2463.

(38) Wang, R.; Liu, X.; Huang, A.; Wang, W.; Xiao, Z.; Zhang, L.; Dai, F.; Sun, D. Unprecedented Solvent-Dependent Sensitivities in Highly Efficient Detection of Metal Ions and Nitroaromatic Compounds by a Fluorescent Barium Metal-Organic Framework. *Inorg. Chem.* **2016**, *55*, 1782-1787.

(39) Shanmugaraju, S.; Mukherjee, P. S. π-Electron rich small molecule sensors for the recognition of nitroaromatics. *Chem. Commun.,* **2015**, *51*, 16014-16032.

(40) Germain, M. E.; Knapp, M. J. Optical explosives detection: from color changes to fluorescence turn-on. *Chem. Soc. Rev.*, **2009**, *38*, 2543-2555.

(41) Germain, M. E.; Vargo, T. R.; Khalifah, P. G.; Knapp, M. J. Fluorescent Detection of Nitroaromatics and 2,3-Dimethyl- 2,3-dinitrobutane (DMNB) by a Zinc Complex: (salophen)Zn. *Inorg. Chem.*, **2007**, *46*, 4422-4429.

(42) He, G.; Peng, H.; Liu, T.; Yang, M.; Zhang, Y.; Fang, Y. A novel picric acid film sensor via combination of the surface enrichment effect of chitosan films and the aggregation-induced emission effect of siloles. *J. Mater. Chem.*, **2009**, *19*, 7347-7353.

(43) Pimienta, V.; Etchenique, R.; Buhse, T. On the Origin of Electrochemical Oscillations in the Picric Acid/CTAB Two-Phase System. *J. Phys. Chem. A*, **2001**, *105*, 10037-10044.

(44) Sylvia, J. M.; Janni, J. A.; Klein, J.; Spencer, K. M. Surface-Enhanced Raman Detection of 2,4-Dinitrotoluene Impurity Vapor as a Marker To Locate Landmines. *Anal. Chem.* **2000**, *72*, 5834-5840.

(45) Wallenborg, S. R.; Bailey, C. G. Separation and Detection of Explosives on a Microchip Using Micellar Electrokinetic Chromatography and Indirect Laser-Induced Fluorescence. *Anal. Chem.* **2000**, *72*, 1872-1878.

(46) Kandpal, M.; Bandela, A. K.; Hinge, V. K.; Rao, V. R.; Rao, C. P. Fluorescence and Piezoresistive Cantilever Sensing of Trinitrotoluene by an Upper-Rim Tetrabenzimidazole Conjugate of Calix[4]arene and Delineation of the Features of the Complex by Molecular Dynamics. *ACS Appl. Mater. Interfaces*, **2013**, *5*, 13448-13456.

(47) Zu, B.; Guo, Y.; Dou, X. Nanostructure-based optoelectronic sensing of vapor phase explosives – a promising but challenging method. *Nanoscale*, **2013**, *5*, 10693-10701.

(48) Toal, S. J.; Trogler, W. C. Polymer sensors for nitroaromatic explosives detection. *J. Mater. Chem.*, **2006**, *16*, 2871-2883.

(49) Vij, V.; Bhalla, V.; Kumar, M. Attogram Detection of Picric Acid by Hexa-peri-Hexabenzocoronene-Based Chemosensors by Controlled Aggregation-Induced Emission Enhancement. *ACS Appl. Mater. Interfaces*, **2013**, *5*, 5373-5380.

(50) Perrin, D. D.; Armarego, W. L. F.; Perrin, D. R. *Purification of Laboratory Chemicals*, Pergamon Press, Oxford, 1980. *Purification of Laboratory Chemicals*, Pergamon Press, Oxford, 1980.

(51) Kumar, G.; Aggarwal, H.; Gupta, R. Cobalt Complexes Appended with para- and meta-Arylcarboxylic Acids: Influence of Cation, Solvent, and Symmetry on Hydrogen-Bonded Assemblies. *Cryst. Growth. Des.* **2013**, *13*, 74-90.

(52) *CrysAlisPro*, Oxford Diffraction Ltd., version 1.171.33.49b (**2009**).

(53) Altomare, A.; Cascarano, G.; Giacovazzo, C.; Guagliardi, A. Completion and refinement of crystal structures with sir92. *J. Appl. Crystallogr.* **1993**, *26*, 343-350.

(54) Sheldrick, G. M. A short history of SHELX. Acta Crystallogr., Sec. A **2008**, 64, 112-122.

(55) Farrugia, L. J. *WinGX version 1.70*, An Integrated System of Windows Programs for the Solution, Refinement and Analysis of Single-Crystal X-ray Diffraction Data; Department of Chemistry, University of Glasgow, **2003**.

(56) Tranchemontagne, D. J.; Mendoza-Cortes, J. L.; O'Keeffe M.; Yaghi, O. M. Secondary building units, nets and bonding in the chemistry of metal–organic frameworks. *Chem. Soc. Rev.,* **2009**, *38,* 1257-1283.

(57) For LnCP **1**, Obs. weight change: 6.7%; Calc.: 6.8% for the loss of two MeOH molecules. For LnCP **2**, Obs. weight change: 7.4%; Calc.: 7.1% for the loss of one MeOH and two water molecules.

(58) Blatov, V. A.; Shevchenko, A. P.; Serezhkin, V. N. Topos 3.2: a new version of the program package for multipurpose crystal-chemical analysis. *J. Appl. Crystallogr.* **2000**, *33*, 1193.
(59) Blatov, V. A.; O'Keefee, M.; Proserpio, D. M. Vertex-, face-, point-, Schlafli-, and Delaney-symbols in nets, polyhedra and tilings: recommended terminology. *CrystEngComm.* **2010**, *12*, 44-48.
(60) A typical fluorescence probe contains a receptor unit (antenna), a luminescence center, and a linker.[19] In the present LnCPs, Eu/Tb ion is the luminescence center, while ligand functions both as a linker and a receptor.
(61) Miller-Chou, B. A.; Koenig, J. L. A review of polymer dissolution. *Prog. Polym. Sci.* **2003**, *28*, 1223-1270.

Table 1. Crystallographic Data Collection and Structure Refinement Parameters for Ligand H_2L and LnCPs 1 and 2.

	H_2L	1	2
Molecular formula	$C_{13}H_{10}N_2O_3$	$C_{41}H_{35}EuN_6O_{11}$	$C_{40}H_{35}TbN_6O_{12}$
Fw	242.23	937.69	945.63
T(K)	293(2)	293(2)	293(2)
Crystal system	Monoclinic	Monoclinic	Monoclinic
Space group	$P2_1/n$	$P2_1/c$	$P2_1/c$
a	13.240 (7)	28.082 (2)	28.0524(12)
b	4.988 (2)	14.6148 (14)	14.7147(9)
c	17.127 (14)	9.7461 (6)	9.7408(4)
α	90	90	90
β	97.56 (6)	96.049 (7)	96.216 (4)
γ	90	90	90

V (Å^3)	1121.3 (12)	3977.7 (6)	3977.2(3)
Z	4	4	4
ρ (g cm^{-3})	1.435	1.566	1.571
F (000)	504.0	1888	1892
μ (Mo Kα) (mm^{-1})	0.104	1.646	1.840
collected reflections	6323	28873	45715
unique reflections	1961(0.1071)	6991(0.1878)	7026(0.1076)
no. of observations	994	4008	5129
Goodness of fit (F^2)	0.988	0.992	1.143
R_1^a, wR_2^b [I >2σ(I)]	0.0772, 0.1721	0.0954, 0.2375	0.0646, 0.1101
R_1^a, wR_2^b [all data]	0.1455, 0.2158	0.1542, 0.3124	0.0939, 0.1190
CCDC No.	1544542	1544543	1544544

[a] $R1 = \Sigma||Fo| - |Fc||/\Sigma|Fo|$; $wR2 = \{\Sigma[w(/Fo/^2 - /Fc/^2)^2]/\Sigma[wFo^4]\}^{1/2}$.

Table 2. Summary of percentage quenching efficiency, Stern-Volmer constant (*Ksv*) and detection limit for LnCP 1 with various nitroaromatics.

Entry	Nitroaromatic	% Quenching Efficiency	*Ksv* (M^{-1})	Detection Limit (µM)
1	Nitrobenzene	98	2.38×10^4	49
2	4-nitrophenol	82	2.54×10^3	66
3	1,3-dinitrobenzene	80	2.01×10^3	88
4	1-nitronapthalene	67	9.88×10^2	90
5	2,4,6-trinitrophenol	64	8.951×10^2	98
6	3,5-dinitrosalicylic acid	52	5.462×10^2	130
7	3,5-dinitrobenzyl chloride	45	4.272×10^2	134
8[a]	Nitrobenzene	96	1.728×10^4	53

[a] Using LnCP ***2***.

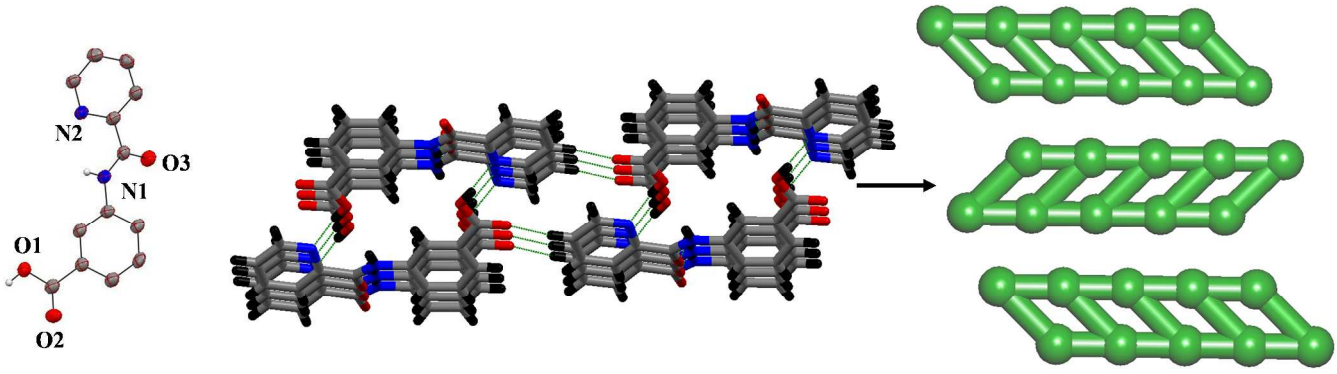

Figure 1. ORTEP representation of the crystal structure of ligand **H_2L** (30% probability level) (left); Color code: blue, N; red, O; gray, C; white, H; H-bonding (COO-H_{acid}…$N_{pyridine}$ and C=O_{acid}…H_{arene}) between individual molecules (middle); and topology of the hydrogen bonded network (right).

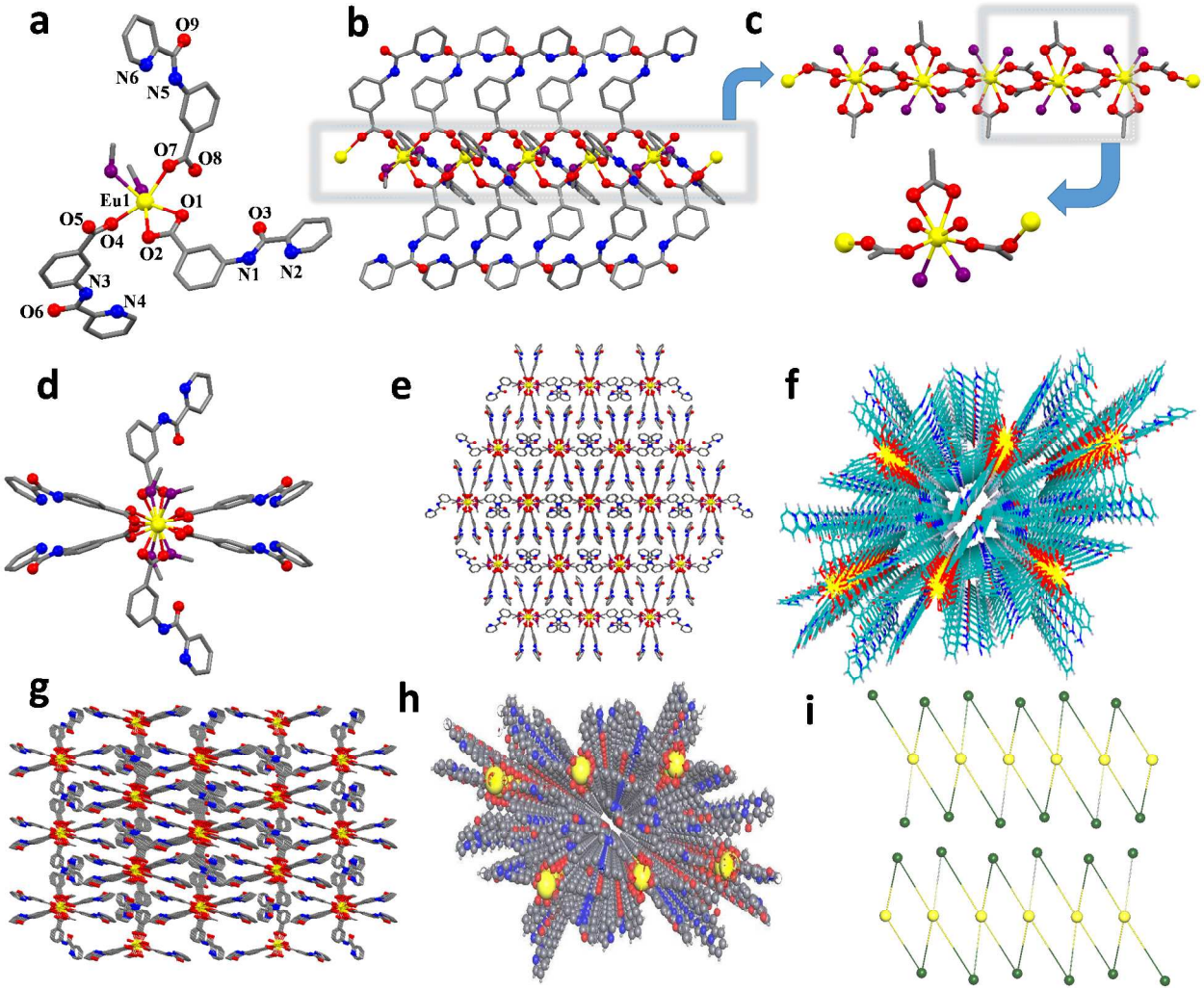

Figure 2. (a) Asymmetric unit cell of LnCP **1**; color code: yellow, Eu; blue, N; red, O; purple, $O_{methanol}$; gray, C; hydrogen atoms are omitted for clarity. (b) Capped sticks representation of **1** along *b*-axis showing exposed amide and pyridyl groups. (c) A closer view of **1** only displaying Eu^{3+} ions and their coordination environment generating a 1D chain (d) A view of 1D chain along the *c*-axis exhibiting exposed amide and pyridyl groups. (e) An extended view of several 1D chains held together by H-bonds as explained in the text in a view along the *c*-axis. (f) A line-diagram perspective view of LnCP **1**. (g) An extended off-set view the along *c*-axis of several 1D chains of LnCP **2**. (h) A ball and stick perspective view of LnCP **2**. (i) A representative topological diagram of LnCP **1** showing Eu atoms as the 4-connected nodes (yellow balls) and ligand as the 2-connected linkers (green balls).

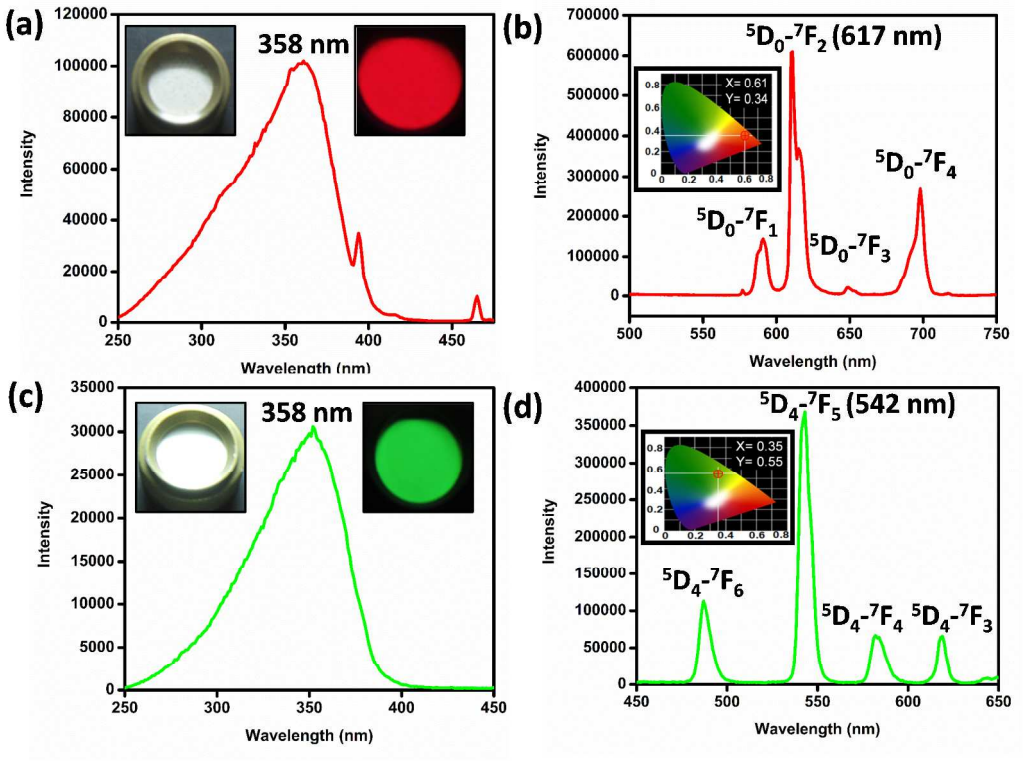

Figure 3. (a) Solid-state excitation spectrum of LnCP **1** at 617 nm whereas insets show powder sample under normal light (left) and UV light of wavelength 350 nm (right). (b) Solid-state emission spectrum of LnCP **1** at excitation wavelength of 358 nm whereas inset shows the CIE chromaticity diagram x = 0.61, y = 0.34. (c) Solid-state excitation spectrum of LnCP **2** at 542 nm whereas insets show powder sample under normal light (left) and UV light of wavelength 350 nm (right). (d) Solid-state emission spectrum of LnCP **2** at excitation wavelength of 358 nm whereas shows the CIE chromaticity diagram x = 0.35, y = 0.55.

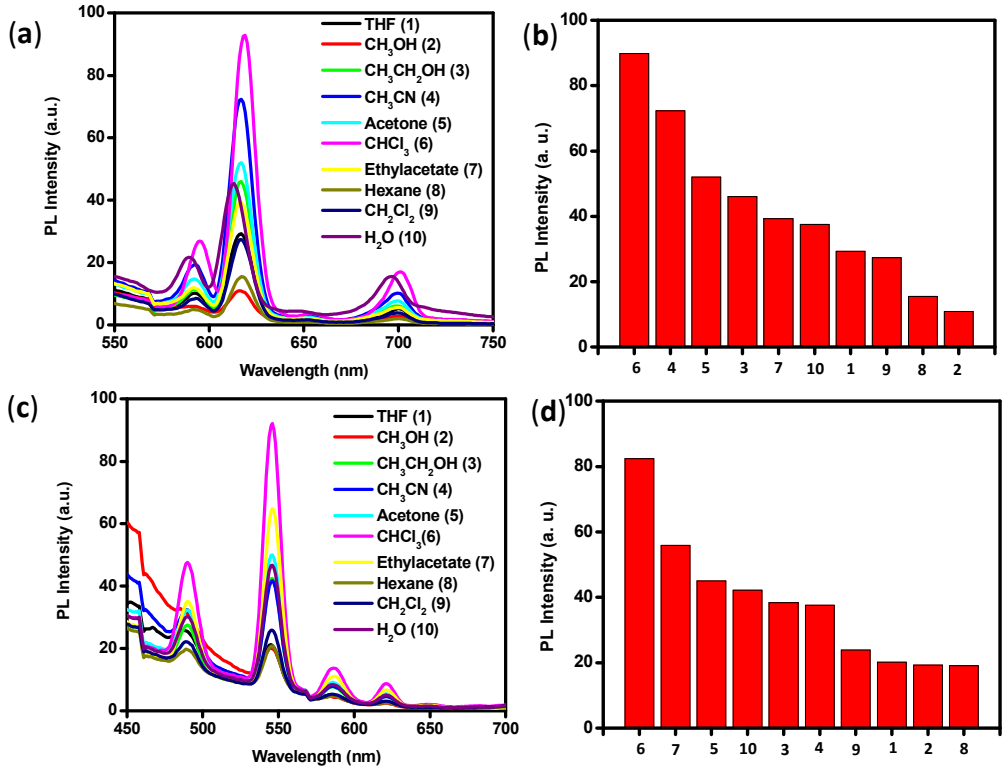

Figure 4. Photoluminescence spectra of LnCPs **1** (a, b) and **2** (c, d) obtained in different solvents as their suspensions. Both LnCPs **1** and **2** show maximum intensity in $CHCl_3$.

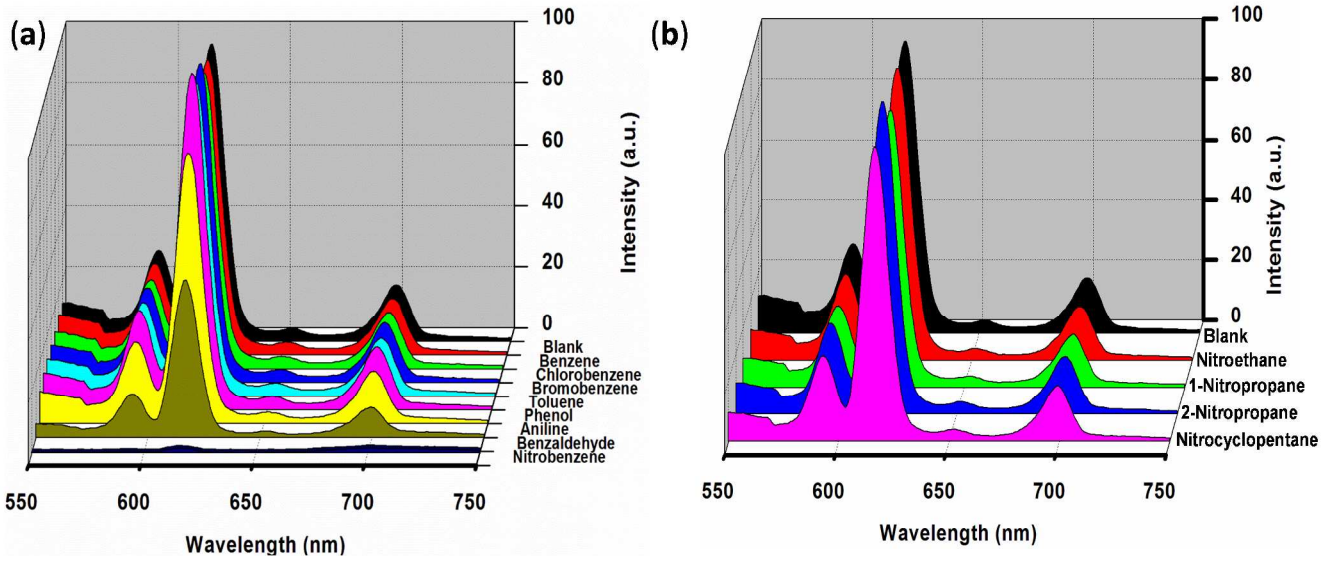

Figure 5. Photoluminescence spectra of LnCP **1** in different solvents as their suspensions: (a) nitroaromatics, and (b) nitroaliphatics.

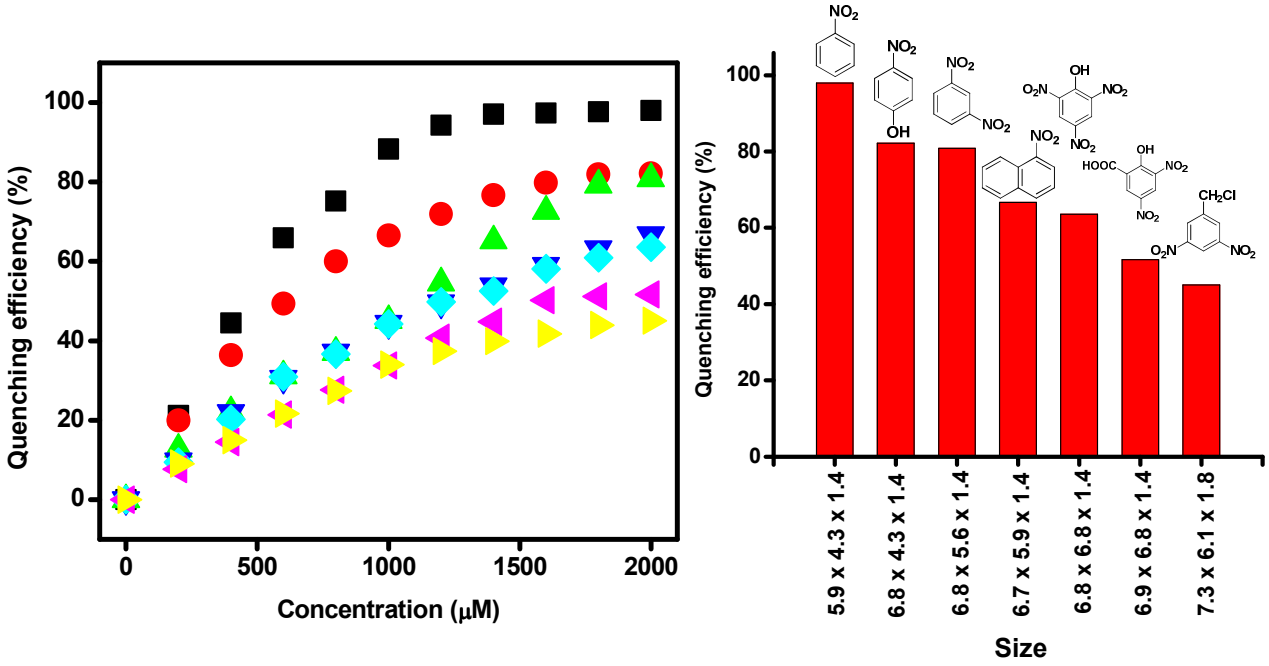

Figure 6. (Left) Photoluminescence quenching efficiency of LnCP **1** in different nitroaromatics varying their μM concentrations: nitrobenzene (■); *para*-nitrophenol (●); 1,3-dinitrobenzene (▲); 1-nitronapthalene (▼), 2,4,6-trinitrophenol (◆); 3,5-dinitrosalicilic acid (◀); 3,5-dinitrobenzylchloride (▶). (Right) Photoluminescence quenching efficiency of LnCP **1** plotted against the molecular dimensions of assorted nitroaromatics.

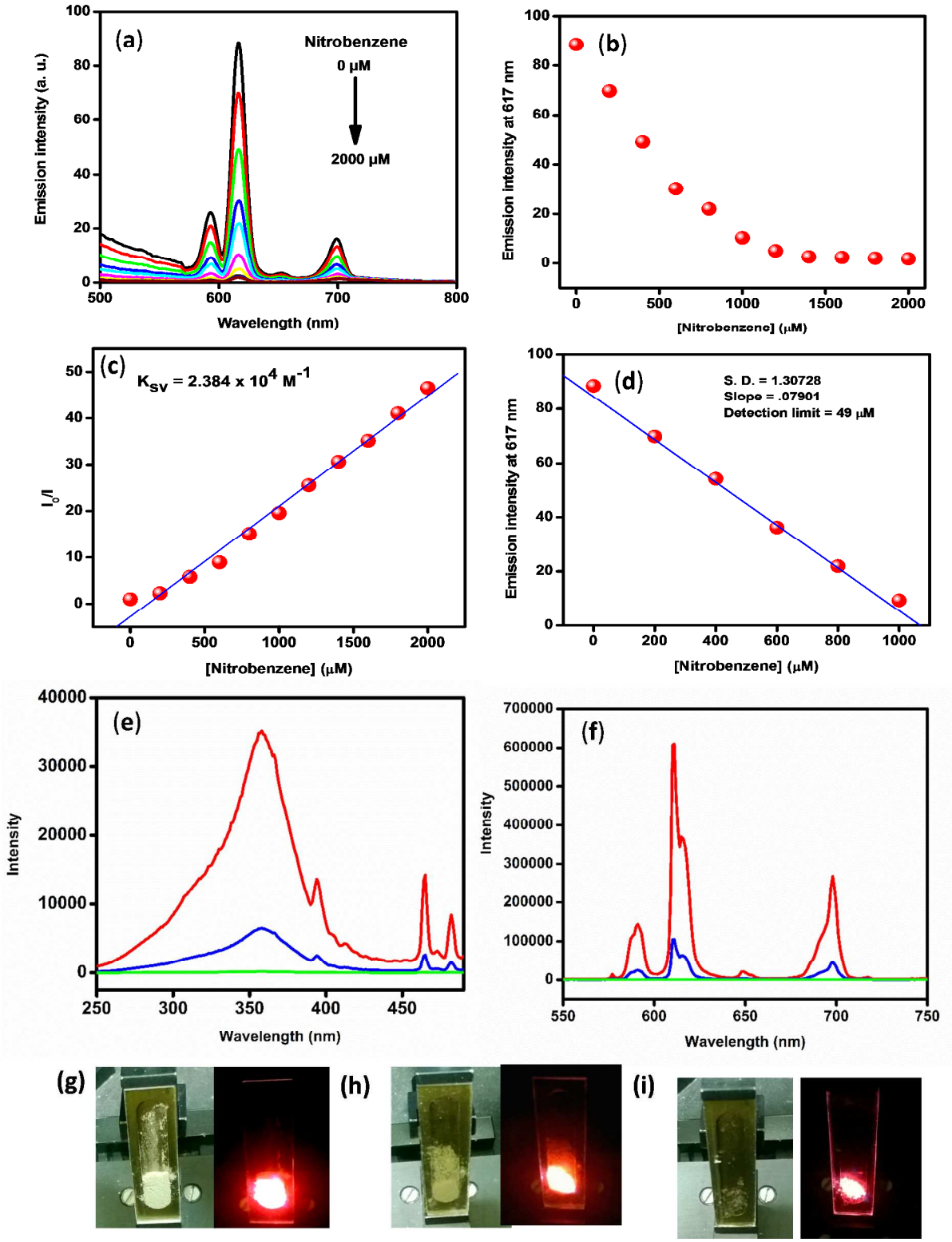

Figure 7. (a) Photoluminescence spectra of LnCP **1** as a $CHCl_3$ suspension after the incremental addition of nitrobenzene. (**b**) Photoluminescence spectra of **1** as a $CHCl_3$ suspension after the incremental addition of nitrobenzene by observing $^5D_0 \rightarrow {}^7F_2$ transition at 617 nm. **(c)** Stern–Volmer analysis of **1** as a function of nitrobenzene concentration. **(d)** A plot for the calculation of detection limit of **1** as a function of nitrobenzene concentration. Solid-state time-dependent (e) excitation spectrum and (f) emission spectrum of LnCP **1** as a result of vapour-phase exposure of nitrobenzene: red trace after 0 h exposure; blue trace after 4 h exposure; and green trace after 12 h exposure. Optical photographs under normal light (left) and UV light of wavelength 350 nm (right) taken at 0 h (red trace in Figure 7 e/f); after 4 h (blue trace in Figure 7 e/f); and after 12 h of vapour-phase exposure of nitrobenzene (green trace in Figure 7 e/f).

For Table of Contents Use Only

Manuscript Title: Lanthanide-based Coordination Polymers for the Size-selective Detection of Nitroaromatics

Authors: Sumit Srivastava,[a] Bipin Kumar Gupta[b] and Rajeev Gupta[*a]

TOC Graphic:

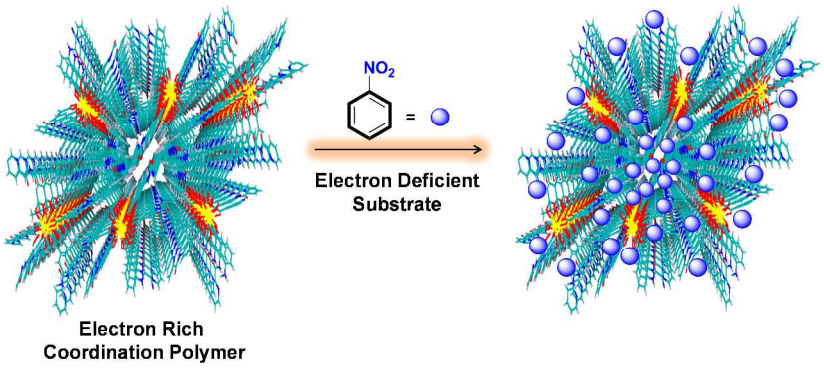

Synopsis: Luminescent coordination polymers, $[Eu(HL)_3(CH_3OH)_2]_n$ (**1**) and $[Tb(HL)_3(CH_3OH)(H_2O)]_n \cdot H_2O$ (**2**), illustrate detection of nitroaromatics in general and size-selective detection of nitrobenzene in particular via a fluorescence Turn-Off mechanism.